Tropical Climate Change Control of the Lower Stratospheric Circulation

Pu Lin*

Program in Atmospheric and Oceanic Sciences, Princeton University

Yi Ming and V. Ramaswamy

Geophysical Fluid Dynamics Laboratory/NOAA

Submitted to *Nature Climate Change*

September 18, 2014

* Corresponding author: Pu.Lin@noaa.gov

The Brewer-Dobson circulation is a major feature of the Earth's climate system, consisting of the slow overturning motion of the stratosphere, with ascent in the tropics and descent in the extratropics [1,2,3]. This airflow impacts the transport and distribution of important climate-influencing constituents in the lower stratosphere including water vapor [4,5], volcanic aerosols [6] and ozone [7,8]. The controls on the changes in this planetary feature and how it is influenced by natural and anthropogenic forcing agents remain unresolved [9]. Here, we use a suite of global climate model simulations, in conjunction with observations-based analysis, to show that the variations in the Brewer-Dobson circulation are attributable to those of the tropical-mean surface temperature. This "bottom-up" control of the global stratospheric circulation operates both on interannual and multi-decadal timescales, and holds for natural and forced variations alike. The circulation change is relatively insensitive to the spatial pattern of the forcings. The invariant influence of the changes in the tropical-mean surface temperature change upon the Brewer-Dobson circulation prevails across timescales and forcings, and constitutes an important attribution element of the changes in the atmosphere due to global climate change.

It would take years for an air parcel in the stratosphere to travel from the tropics to the polar regions following the Brewer-Dobson circulation (BDC) [10], which, albeit much slower than the tropospheric circulation, plays a crucial role in determining the meridional thermal structure of the stratosphere and the concentrations and spatial distributions of stratospheric species [1,2]. Previous modeling studies identified a long-term strengthening trend of the BDC as a result of greenhouse gases (GHGs)-induced warming [11,2] the strengthening is more pronounced for its shallow branch (below 30 hPa) [12]. Yet, the BDC responses to other forcing agents such as anthropogenic aerosols and major volcanic eruptions have not been investigated fully. On

interannual timescales, observations and simulations indicated a more vigorous BDC in the lower stratosphere during the warm phase of the El Niño-Southern Oscillation (ENSO) [13,14]. In this study, we show that the close linkage between the BDC shallow branch and tropical-mean surface temperature (TT) is not unique to ENSO or GHG forcing, and may be applicable to other timescales and externally forced components.

We make use of a 1700-year control simulation conducted with the NOAA/Geophysical Fluid Dynamics Laboratory (GFDL) global climate model CM3 [15]. This model has a fully resolved stratosphere and interactive stratospheric chemistry (see Methods for a detailed description). The strength of the BDC is commonly represented by the mass flux calculated from the Transformed Eulerian Mean (TEM) velocity [16.] We define the shallow branch of the BDC as the upward mass flux across 70 hPa but not reaching 30 hPa, and the deep branch as the mass flux that rises above 30 hPa [12]. We compute the time series of annual mean mass fluxes transported by the shallow and the deep branch of the BDC, as well as annual mean TT averaged over 20°S-20°N.

Figure 1 shows the squared coherence between the strength of the BDC and TT, which measures the correlation between the two time series at different frequencies. The BDC shallow branch shows strong correlations with TT at all frequency, while the coherence between the BDC deep branch and TT is much lower. No appreciable phase difference is found between the BDC shallow branch and TT (not shown).

We also examine a suite of CM3 historical simulations driven by different combination of forcing agents (see Methods for details). Note that this coherence/phase analysis would require a long time series or a large amount of ensembles to resolve the full spectrum, and hence not suitable for historical simulations or reanalysis products. We therefor focus on variations of

two timescales in the following text. The deviations from five-year running means provide a measure of interannual variations, and the averages of consecutive (non-overlapping) five-year segments are used to describe variations on decadal to multi-decadal timescales. Correlation coefficients are calculated between the BDC and TT on these two timescales and summarized in Table 1. Strong correlations are found between the BDC shallow branch and TT on both timescales in all experiments.

On the interannual timescale, the variations of TT is dominated by ENSO with a distinct spatial structure over the central and eastern Pacific, but ENSO may not be the only contributor to the correlation between TT and the BDC shallow branch. A subset of ENSO-neutral years (see Methods for criterion) exhibits similar relationship between the BDC and TT (Fig. 2(a) and Table 1), indicating non-ENSO processes underlying interannual variability behave in a manner similar to ENSO. The correlations between the BDC and TT on the interannual timescale in the forced simulations are similar to those in the unforced control simulations. This is not surprising given that most of the interannual variations are internally generated.

On the decadal to multi-decadal timescales, external forcing agents give rise to variations that are often larger than the internal (unforced) ones. In particular, major volcanic eruptions cause a cooling of the subsequent few years, while anthropogenic GHGs (aerosols) give rise to a secular warming (cooling) trend, which is most appreciable over the second half of the 20th century. Despite very different forcing characteristics, the forced simulations invariantly show the strength of the BDC shallow branch being strongly correlated with TT as shown in Fig. 2(b).

To shed light on the robustness of the CM3 results with regards to model formulation, we repeat the same analysis for CM2.1, an older GFDL coupled model that differs vastly from CM3 in the treatment of several key physical processes as well as stratospheric chemistry [17] (also see

Methods). It also has a much lower model top and coarser resolution in the stratosphere than CM3. As shown in Table 1, results from CM2.1 largely resemble those from CM3.

In addition to model simulations, we also examine the ERA-interim reanalysis data [18] (1979-2012) for possible observational evidence. Due to the relatively short time span of the reanalysis data, we only analyze the interannual variations as shown in Fig. 3. For comparison, we also present results based on the three ensemble members of the AM3, the atmospheric component of the CM3, which runs with the observed sea surface temperatures and all forcing agents. Again, a stronger BDC shallow branch is associated with an increase of TT. Although somewhat weaker than in the model simulation, the correlation between TT and the BDC shallow branch in the reanalysis is statistically significant at the 95% confidence level. The stronger correlation in the model simulations may result from the absence of the quasi-biennial oscillation (QBO), which can modulate the strength of the BDC [19], thus giving rise to interannual variations that are independent of TT.

The correlation coefficients between the BDC deep branch and TT are always lower than those between the shallow branch and TT (Table 1), and the responses of the BDC deep branch to changes of TT are in general weaker (Fig. S1 vs. Fig. 2). The correlation between the BDC deep branch and TT is stronger in CM2.1 than in CM3. We suspect that this may be related to CM2.1's lower model top.

The control of TT on the BDC shallow branch is realized through changing zonal wind structures. Note that it is the zonal winds that modulate the propagation of atmospheric wave activity and the associated wave breaking that drives the stratospheric circulation [16]. Owing to moist convective activities, the tropical surface and free troposphere temperatures are tightly coupled in the sense that the vertical temperature gradient follows approximately the moist

93 adiabatic lapse rate. As a result, when TT varies, greater temperature changes are seen aloft. This
94 vertical amplification of the surface signal in the tropical troposphere results from the release of
95 latent heat associated with moist convective activities [20]. Because the adjustment of moist
96 convection is fast, similar vertical amplification is expected both for interannual and for longer
97 timescales. Indeed, as shown in Fig. S2, at both timescales, the largest temperature responses are
98 seen at around 200 hPa in the tropics, roughly doubling those at the surface. This leads to a
99 change in the meridional temperature gradient in the upper troposphere, and consequently a
100 change in the subtropical zonal winds following the thermal wind balance. More specifically, as
101 the tropical surface warms (cools), the tropics-to-extratropics temperature gradient increases
102 (decreases) in the upper troposphere, and the zonal winds accelerate (decelerate) in the
103 subtropical upper troposphere/lower stratosphere.

104 The zonal wind structure is a key factor in determining the propagation and dissipation of
105 Rossby waves, with the Rossby wave dissipation in the stratosphere being the main driver of the
106 BDC [1,2]. Rossby waves originate from the troposphere with a broad spectra of phase speeds,
107 some of which can propagate to the stratosphere before being absorbed there. It is well-known
108 that the dissipation occurs preferentially at the so-called "critical layers", where the phase speed
109 matches the background zonal wind speed [21]. Typical Rossby waves in the subtropical region
110 reach their critical layers near the tropopause. As the subtropical zonal winds increase, the
111 critical layers tend to move higher, resulting in an upward shift of wave dissipation (Fig. S2).
112 The dissipation of orographic gravity waves, which also contributes to driving the BDC,
113 responds to changes in the subtropical zonal winds in a similar fashion [11,14]. Because the zonal
114 wind changes are largely confined to the lower stratosphere, the wave dissipation at

middle/upper stratosphere is hardly impacted, and the BDC deep branch is therefore insensitive to changes of TT.

This critical layer control mechanism has been invoked to explain the strengthening of the BDC caused by GHGs [22,23] and during the warm phase of ENSO (El Niño) [14]. It is clear that no specific feature of GHG forcing or El Niño is factored into the aforementioned chain of events linking TT to the BDC. A warmer tropical surface is sufficient for initiating them. So, it is not surprising to see that this mechanism holds for the ENSO-neutral years (Fig. S3), as well as for the simulations forced with different external forcings (Figs. S4 and S5). The reanalysis data provide further observational evidence (Fig. S6).

Previous studies have discussed the different responses of the zonal mean circulation to El Niño, greenhouse gases and aerosols, especially in the context of the Hadley circulation [24,25]. Our results, however, suggest that the changes in the BDC shallow branch are largely controlled by the subtropical zonal wind changes associated with the vertical amplification of the tropical surface temperature signal, and the differences in the detailed surface temperature patterns and zonal wind structures remain secondary in this regard. One can rationalize this finding based on the argument that the tropics cannot sustain a strong temperature gradient due to the smallness of the Coriolis parameter (often referred to as the weak temperature gradient approximation) [26]. Then, it follows that whatever temperature structure at the surface would have been smeared at higher altitudes, especially in the upper troposphere. Furthermore, a recent study showed that the surface temperature patterns forced by GHGs and aerosols are very similar [27]. Note that CM3 is one of the models used in that study.

This work demonstrates that despite the persistent uncertainties in the magnitudes and spatial distributions of radiative forcings, one can perceive the variations of the BDC on a wide

range of timescales simply as responsive to the collective effect on the tropical-mean surface temperature. Given the robustness of the underlying physical mechanism, this thinking is likely to be borne out in other models as well. If so, we can gain more confidence in the climate model projection of the long-term trends of stratospheric circulation, composition and the downward impacts on the troposphere and surface by comparing with observed interannual changes.

Methods

GFDL CM3 model simulation

The GFDL CM3 model is a fully coupled atmosphere-ocean climate model with a model top at 0.01 hPa (~86 km) [15]. It has 48 vertical layers, of which 25 layers locates above 100 hPa, and a horizontal resolution of ~200 km. Its tropospheric and stratospheric chemistry scheme is fully interactive. CM3 is one of the Coupled Model Intercomparison Project phase 5 (CMIP5) models in support of the Intergovernmental Panel on Climate Change (IPCC) Fifth Assessment Report. The atmospheric component of CM3 with simpler tropospheric chemistry takes part in the second Chemistry Climate Model Validation Activity (CCMVal-2), which forms the basis of the 2011 WMO ozone assessment 28, and performs as well as or better than its peers in many aspects [9].

We analyze a 1700-year control simulation in which all forcings are fixed at the 1860 (pre-industrial) level, and a suite of historical simulations forced with different forcing combinations. These historical simulations include: all forcing runs (AllForc), natural foricng runs (Natural), anthropogenic forcing runs (Anthro), anthropogenic aerosol forcing only runs (Aerosol), and greenhouse gases and stratospheric ozone only runs (WMGGO3). These historical experiments are configured following the CMIP5 guidelines [29]. Each historical experiment consists of three ensemble members and covers 1860-2004. In our analysis, each member is treated as an independent sample.

GFDL CM2.1 simulation

CM2.1 is an earlier generation GFDL coupled model [17], one of the CMIP3 models used for the IPCC Fourth Assessment Report. It has 24 levels in the atmosphere with a model top at 3 hPa

(~40 km). Its horizontal resolution is ~200 km. CM2.1 does not include interactive chemistry in the stratosphere, and the stratospheric ozone concentration is prescribed. Nor does it consider aerosol-cloud interactions.

We analyze the CM2.1 historical simulations (1861-2000) in three experiments: Natural, Aerosol and WMGGO3. Each experiment consists of three ensemble members.

Diagnosing the BDC in model simulations

Because the BDC is a very slow Lagrangian circulation, direct measurement of its strength is difficult. It is commonly approximated by the diabatic circulation (which dynamically balances the diabatic heating in the meridional plane), or the residual circulation represented by the transformed Eulerian mean (TEM) stream function Ψ^* [16]. The strength of the BDC is then represented by the mass flux transported by the TEM velocity. The TEM velocity can be calculated following its definition [16] or the "downward control principle" [30], both of which inconveniently require knowledge of high frequency data (four times daily or higher). In this study, we diagnose TEM velocity by solving the TEM thermodynamic equation, which only requires data of monthly frequency.

The TEM thermodynamic equation is:

$$\overline{\theta}_t - (a\rho_0 \cos\phi\,)^{-1}\,\Psi_z^*\overline{\theta}_\phi + (a\rho_0 \cos\phi)^{-1}\,\Psi_\phi^*\overline{\theta}_z - \overline{Q} = -\rho_0^{-1}[\rho_0(\overline{v'\theta'}\,\frac{\overline{\theta}_\phi}{a\overline{\theta}_z} + \overline{w'\theta'})]_z \qquad (1)$$

in which over-bars denote zonal means, primes denote deviation from zonal means, and subscripts denote derivatives. Q is the diabatic heating rate, and other variables follow their conventional definitions. The right-hand side of the above equation is usually small and omitted, and all variables on the left-hand side except Ψ^* can be read from monthly mean model output. Straightforward integration of this equation is not possible due to numerical instabilities.

Previous studies employed iterative methods to solve this equation, which do not guarantee the convergence to the solution [31,32]. Following the study by Santee and Crisp [33], we first take the derivative of the entire equation with respect to ϕ. The resulting equation can be easily solved using the finite differential method with the boundary condition $\Psi^*=0$ at poles. Mass flux is calculated from monthly Ψ^* and then averaged annually.

We further diagnose wave forcing *X* from the TEM momentum equation:

$$\overline{u}_t - (\rho_0 \cos\phi)^{-1}\Psi_z^*\left[(a\cos\phi)^{-1}(\overline{u}\cos\phi)_\phi - f\right] + (\rho_0 a\cos\phi)^{-1}\Psi_\phi^*\overline{u}_z = X \qquad (2)$$

The dissipation of Rossby waves in the stratosphere deposits easterly momentum and decelerates the mean flow there. Stronger wave dissipation is indicated by a more negative *X* and would lead to a stronger BDC. Note that *X* includes the contributions from both resolved and subgrid waves, and is equivalent to the divergence of the Eliassen-Palm (EP) flux for resolved waves [16].

Definition of ENSO-neutral years

We calculate the Nino3.4 index [34], and define the ENSO-neutral years as those in which the magnitude of the annual mean Nino3.4 index is less than 0.2 ℃. Using other ENSO indices yields similar results.

Reanalysis data

We compare the historical simulation with ERA-interim reanalysis data [18] for 1979-2009. The TEM velocity from ERA-interim reanalysis is calculated using 6-hourly data following its definition, and the wave forcing *X* is calculated using equation (2). A recent study found that the climatology of the BDC is well represented in this reanalysis dataset [35].

212 # References

1. Holton, J. R. *et al.*, Stratosphere-troposphere exchange. *Rev. Geophys.* **33**, 403-439 (1995).

2. Butchart, N., The Brewer-Dobson circulation. *Rev. Geophys.* **52** (2), 157-184 (2014).

3. Randel, W. J. & Jensen, E. J., Physical processes in the tropical tropopause layer and their roles in a changing climate. *Nat. Geosci.* **6**, 169-176 (2013).

4. Solomon, S. *et al.*, Contribution of stratospheric water vapor to decadal changes in the rate of global warming. *Science* **327**, 1219-1223 (2010).

5. Dessler, A. E., Schoeberl, M. R., Wang, T., Davis, S. M. & Rosenlof, K. H., Stratospheric water vapor feedback. *P. Nat. Acad. Sci. U.S.A.* **110** (45), 18087-18091 (2013).

6. Robert, A., Volcanic eruptions and climate. *Rev. Geophys.* **38**, 191-219 (2000).

7. Forster, P. M. D. & Shine, K. P., Radiative forcing and temperature trends from stratospheric ozone changes. *J. Geophys. Res.* **102**, 10841-10855 (1997).

8. Polvani, L. M., Waugh, D. W., Correa, G. J. P. & Son, S. W., stratospheric ozone depletion: the main driver of the twentieth-century atmospheric circulation changes in the Southern Hemisphere. *J. Clim.* **24**, 795-812 (2011).

9. SPARC CCMVal, SPARC Report No. 5 Report No. WCRP-30, WMO/TD-No. 40, 2010.

10. Waugh, D. & Hall, T., Age of stratospheric air: theory, observations and models. *Rev. Geophys.* **40** (4), 1-1 - 1-26 (2002).

11. Butchart, N. *et al.*, Chemistry-Climate Model simulations of twenty-first century stratospheric climate and circulation chagnes. *J. Clim.* **23**, 5349-5374 (2010).

12. Lin, P. & Fu, Q., Changes in various branches of the Brewer-Dobson circulation from an ensemble of chemistry climate models. *J. Geophys. Res.* **118**, 73-84 (2013).

13. Randel, W. J., Garcia, R. R., Calvo, N. & Marsh, D., ENSO influence on zonal mean temperature and ozone in the tropical lower stratosphere. *Geophys. Res. Lett.* **36**, L15822 (2009).

14. Calvo, N., Garcia, R. R., Randel, W. J. & Marsh, D. R., Dynamical mechanism for the increase in tropical upwelling in the lowermost tropical stratosphere during warm ENSO events. *J. Atmos. Sci.* **67**, 2331-2340 (2010).

15. Donner, L. J. *et al.*, The dynamical core, physical parameterizations, and basic simulation characteristics of the atmospheric component AM3 of the GFDL Global Coupled Model CM3. *J. Clim.* **24**, 3484-3519 (2011).

16. Andrews, D. G., Holton, J. R. & Leovy, C. B., *Middle Atmosphere Dynamics* (Academic Press, San Diego, CA, 1987).

17. Delworth, T. L. *et al.*, GFDL's CM2 global coupled climate models. Part I; formulation and simulation characteristics. *J. Clim.* **19**, 643-674 (2006).

18. Dee, D. P. *et al.*, The EAR-Interim reanalysis: configuration and performance of the data assimilation system. *Q. J. Roy. Meteorol. Soc.* **137**, 553-597 (2011).

19. Holton, J. R. & Tan, H.-C., The influence of the equatorial quasi-biennial oscillation on the global circulation at 50 mb. *J. Atmos. Sci.* **37**, 2200-2208 (1980).

20. Ramaswamy, V. *et al.*, in *Temperature trends in the lower atmosphere: steps for understanding and reconciling differences*, edited by Karl, T. R., Hassol, S. J., Miller, C. D. & Murray, W. L. (2006).

21. Randel, W. J. & Held, I. M., Phase speed spectra of transient eddy fluxes and critical layer absorption. *J. Atmos. Sci.* **48**, 6888-6897 (1991).

22. Garcia, R. R. & Randel, W. J., Acceleration of the Brewer-Dobson circulation due to increase in greenhouse gases. *J. Atmos. Sci.* **65**, 2731-2739 (2008).

23. Shepherd, T. G. & McLandress, C., A robust mechanism for strengthening of the Brewer-Dobson circulation in response to climate change: critical-layer control of subtropical wave breaking. *J. Atmos. Sci.* **68**, 784-797 (2011).

24. Lu, J., Chen, G. & Frierson, D. M. W., Response of the zonal mean atmospheric circulation to El Nino versus global warming. *J. Clim.* **21**, 5835-5851 (2008).

25. Ming, Y. & Ramaswamy, V., A model investigation of aerosol-induced changes in tropical circulation. *J. Clim.* **24**, 5125-5133 (2011).

26. Sobel, A. H., Nilsson, J. & Polvani, L. M., The weak temperature gradient approximation and balanced tropical moisture wave. *J. Atmos. Sci.* **58**, 3650-3665 (2001).

27. Xie, S.-P., Lu, B. & Xiang, B., Similar spatial patterns of climate responses to aerosol and greenhouse gas changes. *Nat. Geosci.* **6**, 828-832 (2013).

28. WMO, Global Ozone Research and Monitoring Project Report No. 52, 2011.

29. Taylor, K. E., Stouffer, R. J. & Meehl, G. A., An overview of CMIP5 and the experiment design. *Bull. Am. Meteor. Soc.* **93**, 485-498 (2012).

30. Haynes, P. H., Marks, C. J., McIntyre, M. E., Shepherd, T. G. & Shine, K. P., On the downward conrol of extratropical diabatic circulations by eddy-induced mean zonal forces. *J. Atmos. Sci.* **48**, 651-679 (1991).

31. Solomon, S., Kiehl, J. T., Garcia, R. R. & Grose, W., Tracer transport by the diabatic circulation deduced from satellite observations. *J. Atmos. Sci.* **43**, 1603-1617 (1986).

32. Rosenlof, K. H., Seasonal cycle of the residual mean meridional circulation in the stratosphere. *J. Geophys. Res.* **100**, 5173-5191 (1995).

33. Santee, M. L. & Crisp, D., Diagnostic calculations of the circulation in the Martian atmosphere. *J. Geophys. Res.* **100**, 5465-5484 (1995).

34. Trenberth, K. E. & Stepaniak, D. P., Indices of El Nino evolution. *J. Clim.* **14**, 1697-1701 (2001).

35. Seviour, W. J. M., Butchart, N. & Hardiman, S. C., The Brewer-Dobson circulation inferred from ERA-Interim. *Q. J. Roy. Meteor. Soc.* **138**, 878-888 (2012).

214

215

Supplementary Information

Supplementary materials are attached.

Acknowledgements

We thank Drs. Isaac Held and R. John Wilson for critical discussions and reading of the manuscript. This paper was prepared by Pu Lin under award NA08OAR4320752 from the National Oceanic and Atmospheric Administration, U.S. Department of Commerce. The statements, findings, conclusions, and recommendations are those of the author(s) and do not necessarily reflect the views of the National Oceanic and Atmospheric Administration, or the U.S. Department of Commerce.

Author Contributions

P. L. and Y. M. designed the analysis; P. L. performed the analysis. All authors discussed the results and wrote the paper.

Author Information

Correspondence should be addressed to Pu Lin (Pu.Lin@noaa.gov).

Tables

Table 1 **Correlation coefficients between the strength of the Brewer-Dobson circulation and the tropical-mean surface temperature.** Correlations are calculated for variations of interannual and decadal to multi-decadal timescales (see text for definitions). For the interannual timescale, correlations are also calculated using subsets of ENSO-neutral years with results shown in parentheses.

		Shallow Branch		Deep Branch	
		Interannual	Decadal to Multi-decadal	Interannual	Decadal to Multi-decadal
ERA-i		0.54	-	-0.18	-
AM3	AllForc	0.64	-	0.57	-
		0.63	-	0.23	-
		0.60	-	0.30	-
CM3	Control	0.68 (0.56)	0.59	0.27 (0.25)	0.18
	AllForc	0.75 (0.59)	0.80	0.23 (0.29)	0.49
	Natural	0.67 (0.46)	0.83	0.31 (0.24)	0.36
	Anthro	0.66 (0.49)	0.86	0.34 (0.31)	0.73
	Aerosol	0.67 (0.50)	0.96	0.31 (0.25)	0.58
	WMGGO3	0.67 (0.59)	0.98	0.22 (0.18)	0.90
CM2.1	Natural	0.75 (0.66)	0.70	0.48 (0.43)	0.09
	Aerosol	0.71 (0.67)	0.60	0.60 (0.69)	0.31
	WMGGO3	0.78 (0.54)	0.95	0.64 (0.42)	0.91

Figure Legends

Fig.1 **Squared coherence between the strength of the Brewer-Dobson circulation and the tropical-mean surface temperature.** Black line for the shallow branch of the Brewer-Dobson circulation, and red line for the deep branch. Results are based on the 1700-year pre-industrial control simulation. Coherence is estimated using Welch's averaged modified periodogram method with a Hamming window of 32 years.

Fig.2 **Scatter plot of the strength of the Brewer-Dobson circulation shallow branch versus the tropical mean surface temperature in CM3.** (a) for the interannual timescale from the control simulation. ENSO-neutral years are marked by red dots. (b) for the decadal to multi-decadal timescale from the control and historical forced simulations. Climatological means are removed.

Fig. 3 **Scatter plot of the strength of the Brewer-Dobson circulation shallow branch versus the tropical-mean surface temperature during the recent decades from the reanalysis and model simulations.** (a) from the ERA interim reanalysis for 1981-2010. (b) from the three ensemble member of AM3 AllForc simulation for 1974-2010. Only the interannual timescale is considered here. Correlation coefficients are given on the lower-right corner of each panel.

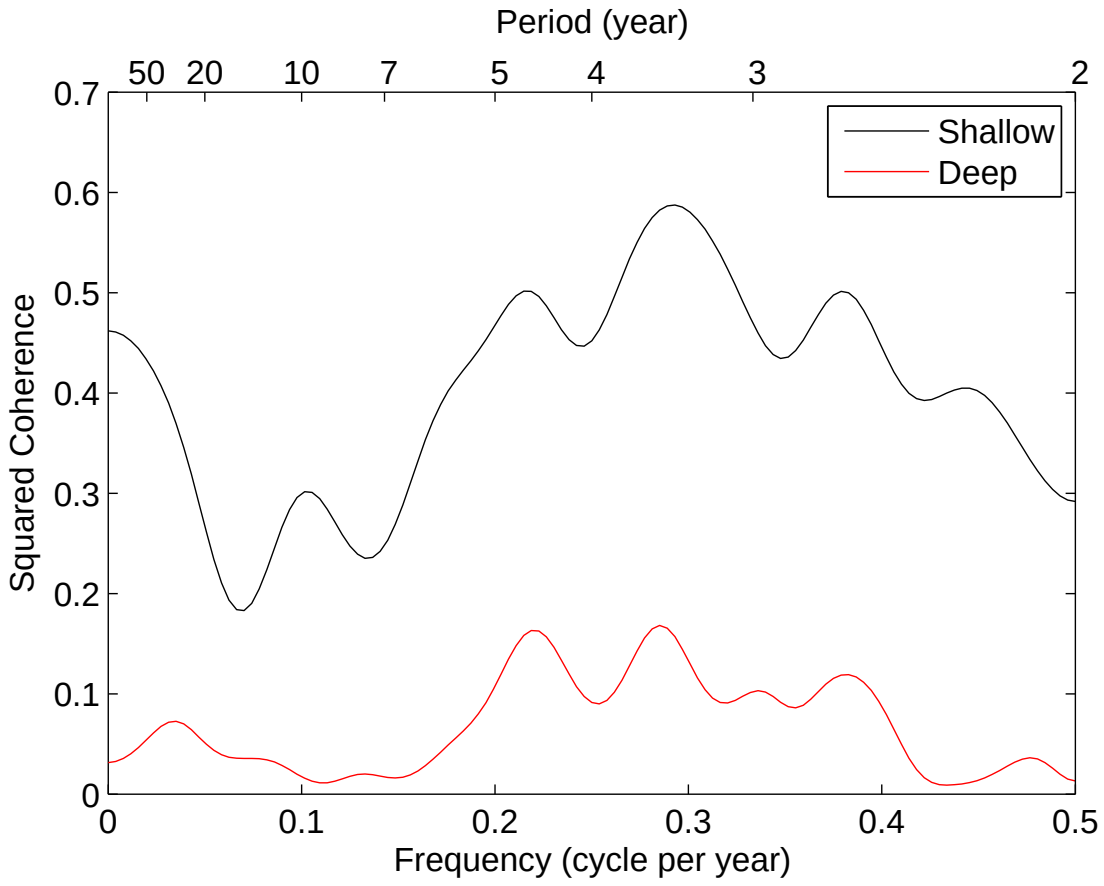

Figure 1: **Squared coherence between the strength of the Brewer-Dobson circulation and the tropical mean surface temperature.** Black line for the shallow branch of the Brewer-Dobson circulation, and red line for the deep branch. Results are based on the 1700-year pre-industrial control simulation. Coherence is estimated using Welch's averaged, modified periodogram method with a Hamming window of 32 years.

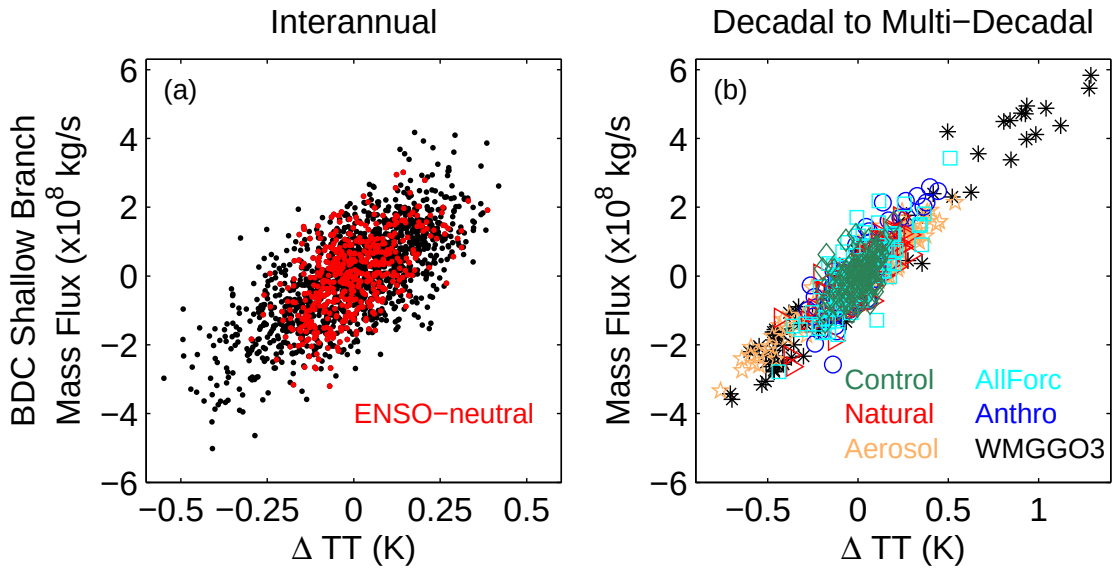

Figure 2: **Scatter plot of the strength of the Brewer-Dobson circulation shallow branch versus the tropical mean surface temperature in CM3.** (a) for interannual timescales from the control simulation. ENSO-neutral years are marked by red dots. (b) for the decadal to multi-decadal timescale from the control simulations and historical forced simulations. Climatological mean is removed.

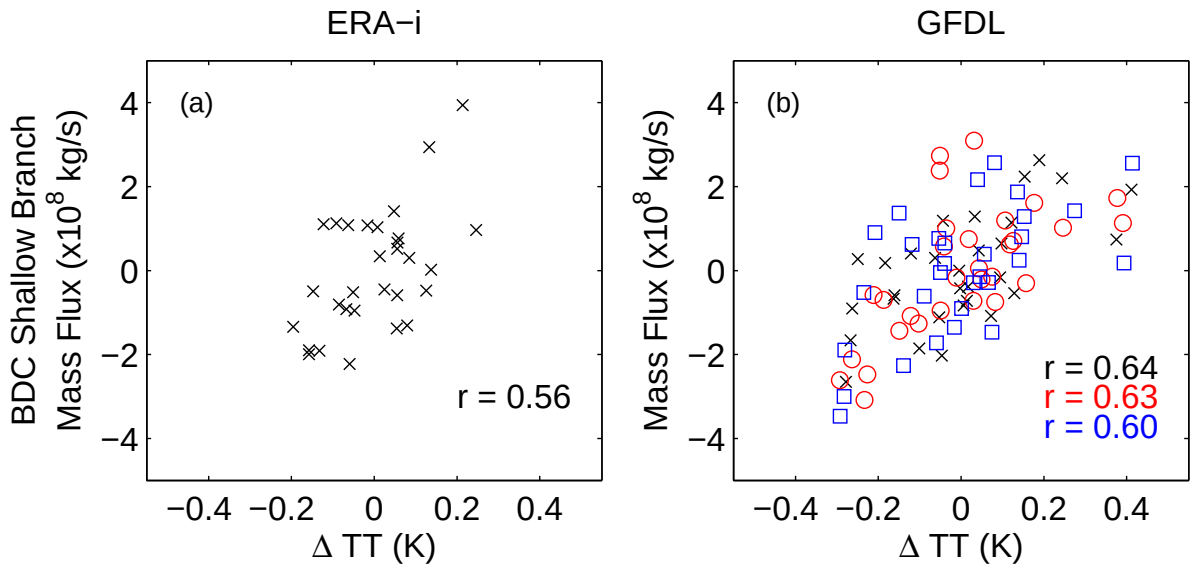

Figure 3: **Scatter plot of the strength of the Brewer-Dobson circulation shallow branch versus tropical mean surface temperature during the recent decades from the reanalysis and the model simulations.** (a) from the ERA interim reanalysis for 1981-2010. (b)from the three ensemble member of AM3 AllForc simulation for 1974-2003. Only the interannual timescale is considered here. Correlation coefficients are given on the lower-right corner of each panel.

Tropical Climate Change Control of the Lower Stratospheric Circulation: Supplementary Materials

Pu Lin

*Program in Atmospheric and Oceanic Sciences, Princeton University.**

Yi Ming and V. Ramaswamy

Geophysical Fluid Dynamics Laboratory / NOAA

(Dated: September 18, 2014)

* To whome correspondence should be addressed:

Pu.Lin@noaa.gov

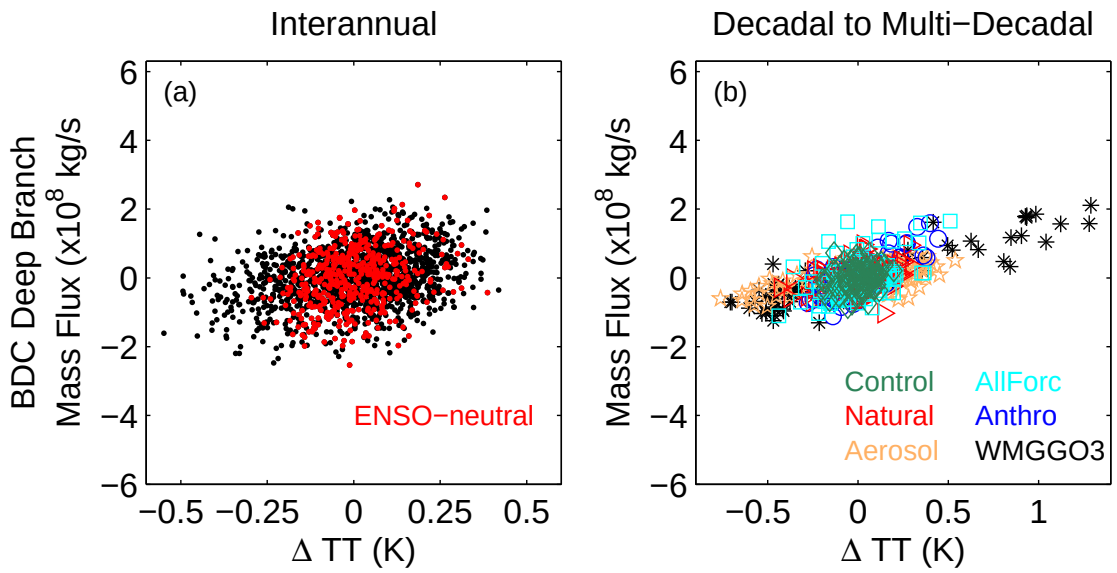

Fig. S1 **Scatter plot of the Brewer-Dobson deep branch versus the tropical-mean surface temperature in CM3** (a) for the interannual anomalies from the control simulations. ENSO-neutral years are maked by read dots. (b) for the multi-decadal timescale from the control simulation and historical forced simulations. Climatological mean is removed.

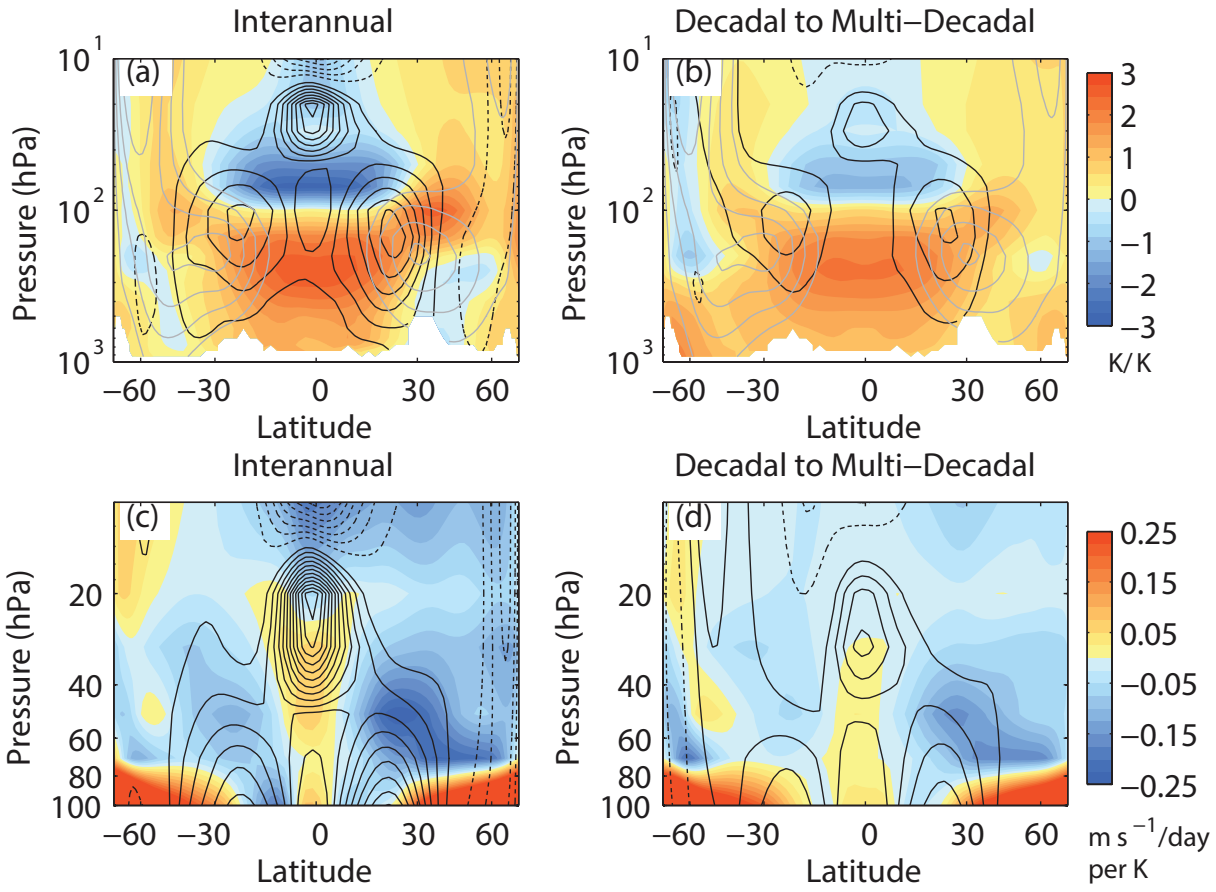

Fig. S2 **Response of zonal mean temperature, zonal wind and wave forcing to changes of the tropical mean surface temperature** (a) and (b) Regression of zonal mean temperature (color shading) and zonal wind (black contours) upon tropical mean surface temperature from the control simulation. Contour interval for zonal wind regression is 1.5 m/s/K, with negative contours in dashed lines, and the zero contour is omitted. The climatology of zonal mean zonal wind (light gray contours) is also plotted for comparison. Contour interval for zonal wind climatology is 7.5 m/s. Zero wind and easterlies are omitted for clarity. (c) and (d) Regression of zonal mean zonal wind (contours) and wave forcing (color shading) upon the tropical mean surface temperature from the control simulation. See Methods for the definition of the wave forcing. Contour interval for zonal wind regression is 1 m/s/K, with negative contours in dashed lines and the zero contour is omitted. (a) and (c) for the interannual timescale, (b) and (d) for the decal to multi-decadal timescale.

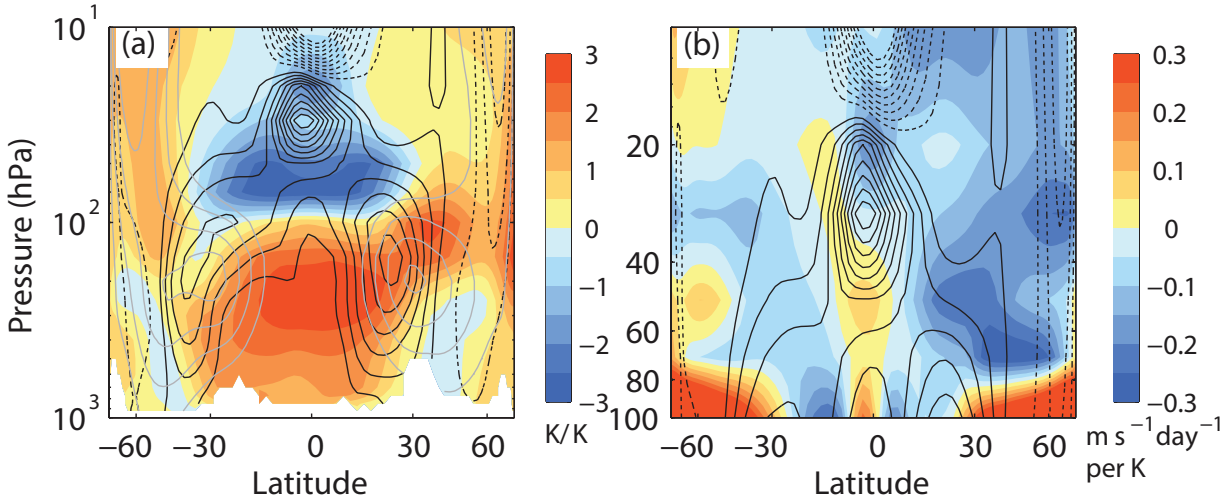

Fig. S3 **Response to changes in tropical mean surface temperature on interannual timescales using ENSO-neutral years from the control simulation.** (a) Regression of zonal mean temperature (color shading) and zonal wind (black contours) upon the tropical mean surface temperature. Contour interval for zonal wind regression is 1.5 m/s/K, with negative contours in dashed lines, and the zero contour is omitted. Zonal mean zonal wind climatology is plotted in gray contours for comparison. Contour interval for zonal wind climatology is 7.5 m/s, and only westerlies are plotted for clarity. (b) Regression of zonal mean zonal wind (contours) and wave forcing (color shading) upon the tropical mean surface temperature. Contour interval is 1.5m/s/K, with negative contours in dashed lines, and the zero contour is omitted.

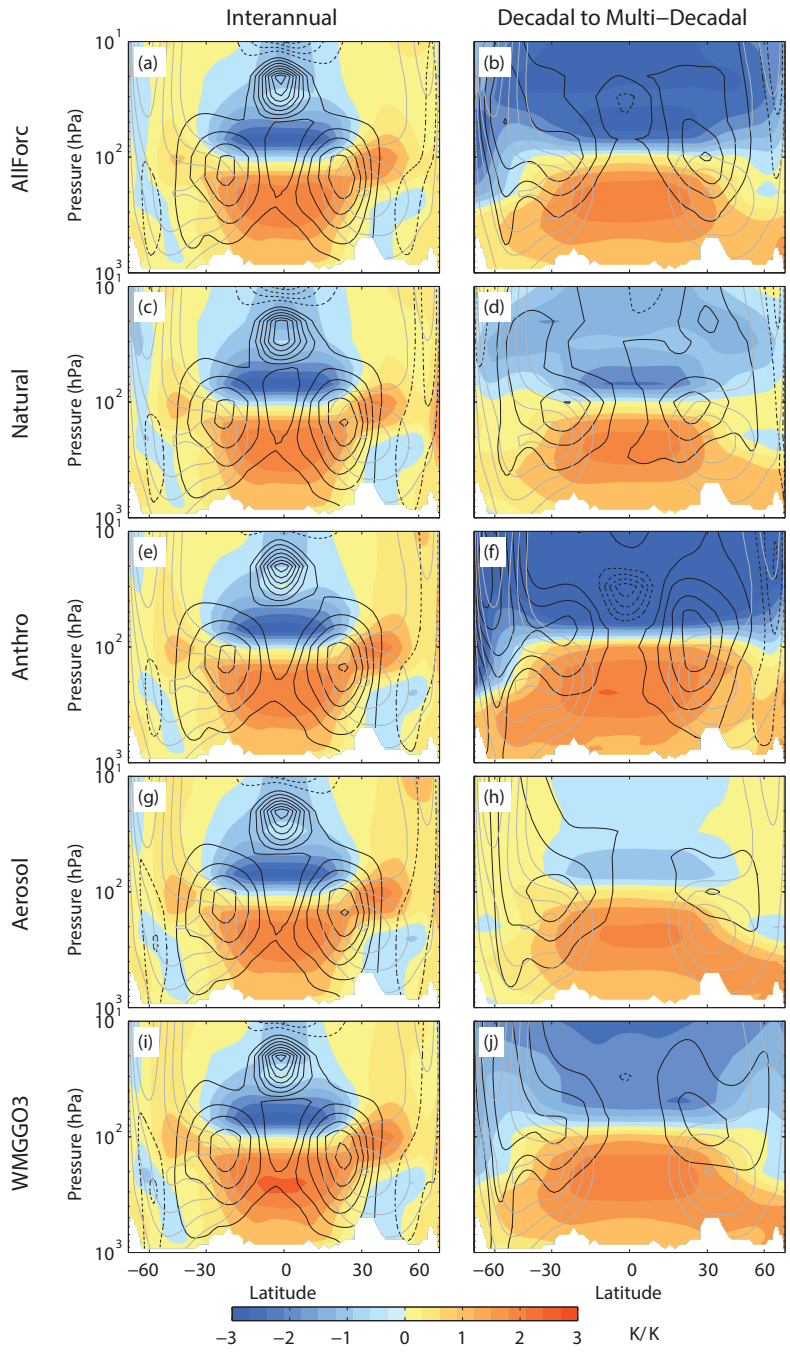

Fig. S4 **Response of zonal mean temperature and zonal wind to changes in the tropical mean surface temperature in forced simulations.** Regression of zonal mean temperature (color shading) and zonal wind (black contours) upon the tropical-mean surface temperature on (left) interannual timescales and (right) decadal to multi-decadal timescales. Contour interval for zonal wind regression is 1.5 m/s/K for interannual timescales and 0.75 m/s/K for decadal to multi-decadal timescales, with negative contours in dashed lines, and the zero contour is omitted. The climatology of zonal mean zonal wind (light gray contours) is also plot for comparison. Contour interval for zonal wind climatology is 7.5 m/s. Zero wind and easterlies are omitted for clarity.

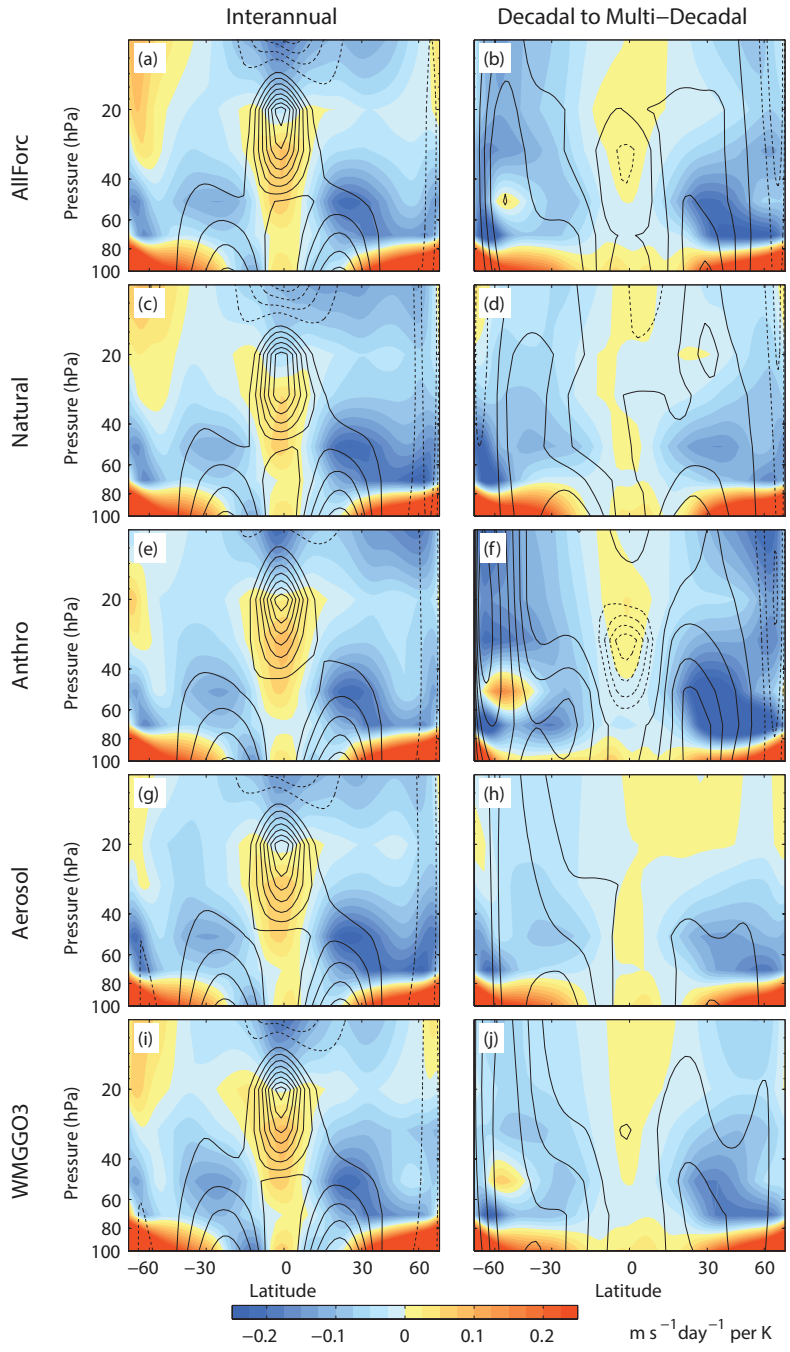

Fig. S5 **Response of zonal mean zonal wind and wave forcing to changes in the tropical mean surface temperature in forced simulations.** Regression of zonal mean zonal wind (contours) and wave forcing (color shading) upon the tropical mean surface temperature from the control simulation on (left) interannual timescales and (right) decadal to multi-decadal timescales. See Methods for the definition of the wave forcing. Contour interval for zonal wind regression is 1.5 m/s/K for interannual timescales and 0.75 m/s/K for decadal to multi-decadal timescales, with negative contours in dashed lines and the zero contour is omitted.

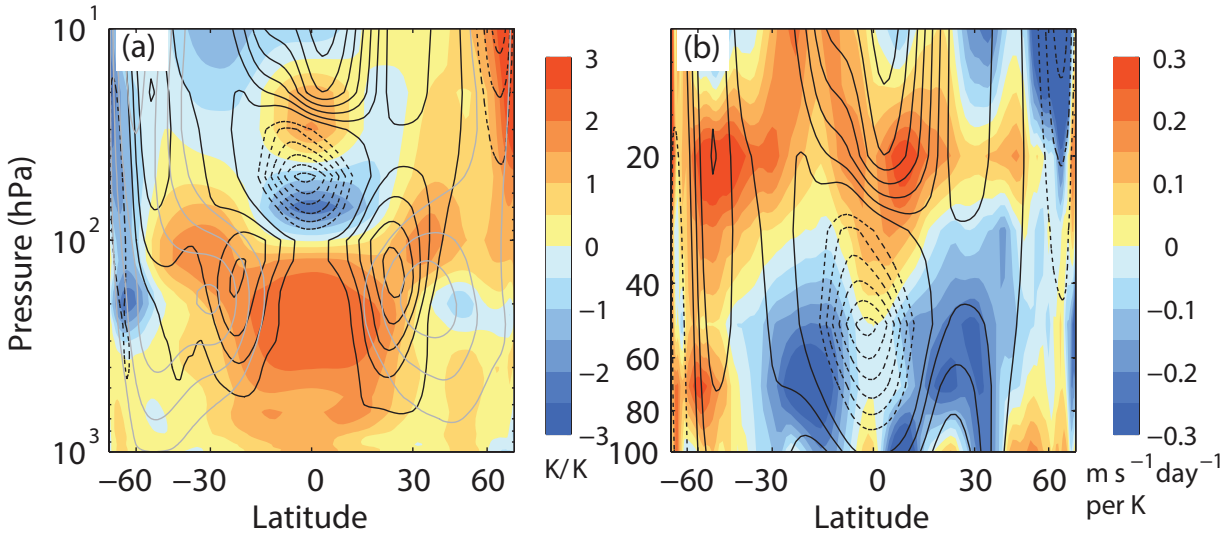

Fig. S6 **Response to changes in tropical mean surface temperature on interannual timescales in reanalysis.** (a) Regression of zonal mean temperature (color shading) and zonal wind (black contours) upon the tropical mean surface temperature from ERA interim reanalysis for 1981-2010. Contour interval for zonal wind regression is 1.5 m/s/K, with negative contours in dashed lines, and the zero contour is omitted. Zonal mean zonal wind climatology is plotted in gray contours for comparison. Contour interval for zonal wind climatology is 7.5 m/s, and only westerlies are plotted for clarity. (b) Regression of zonal mean zonal wind (contours) and wave forcing (color shading) upon the tropical mean surface temperature. Contour interval is 1.5 m/s/K, with negative contours in dashed lines, and the zero contour is omitted.